Published in final edited form as:
Magn Reson Med. 2008 May ; 59(5): 1079–1089. doi:10.1002/mrm.21563.

High b-value q-space Diffusion Weighted MRI of the Human Cervical Spinal Cord *in vivo*: Feasibility and Application to Multiple Sclerosis

Jonathan A.D. Farrell[1,2,3], **Seth A. Smith**[1,2], **Eliza M. Gordon-Lipkin**[4], **Daniel S. Reich**[1,4], **Peter A. Calabresi**[4], and **Peter C.M. van Zijl**[1,2,3]

[1]Russell H. Morgan Department of Radiology and Radiological Science, Johns Hopkins University School of Medicine, Baltimore, Maryland, USA.

[2]F.M. Kirby Research Center for Functional Brain Imaging, Kennedy Krieger Institute, Baltimore, Maryland, USA.

[3]Department of Biophysics and Biophysical Chemistry, Johns Hopkins University School of Medicine, Baltimore, Maryland, USA.

[4]Department of Neurology, Johns Hopkins University School of Medicine, Baltimore, Maryland, USA.

Abstract

Q-space analysis is an alternative analysis technique for diffusion weighted imaging (DWI) data in which the probability density function (PDF) for molecular diffusion is estimated without the need to assume a Gaussian shape. Although used in the human brain, q-space DWI has not yet been applied to study the human spinal cord *in vivo*. Here we demonstrate the feasibility of performing q-space imaging in the cervical spinal cord of eight healthy volunteers and four patients with multiple sclerosis. The PDF was computed and water displacement and zero-displacement probability maps were calculated from the width and height of the PDF, respectively. In the dorsal column white matter, q-space contrasts showed a significant ($p<0.01$) increase in the width and a decrease in the height of the PDF in lesions, the result of increased diffusion. These q-space contrasts, which are sensitive to the slow diffusion component, exhibited improved detection of abnormal diffusion compared to perpendicular apparent diffusion constant measurements. The conspicuity of lesions compared favorably with magnetization transfer (MT) weighted images and quantitative CSF-normalized MT measurements. Thus q-space DWI can be used to study water diffusion in the human spinal cord *in vivo* and is well suited to assess white matter damage.

Keywords

diffusion; q-space; spinal cord; multiple sclerosis

INTRODUCTION

In white matter (WM), the axonal membrane and myelin sheath present barriers to water displacement, resulting in anisotropic diffusion (1–4). WM damage is known to affect tissue microstructure and diffusion weighted MRI (DWI) has been used to measure changes in

Corresponding Author: Peter C.M. van Zijl, PhD, F.M. Kirby Research Center for Functional Brain Imaging, Kennedy Krieger Institute, 707 N. Broadway, Baltimore, MD 21205, Work: 443-923-9511, Fax: 443-923-9505, pvanzijl@jhu.edu.

diffusion properties (both parallel and perpendicular to WM fiber bundles) in a number of WM diseases in humans (5) as well as animal models of myelin deficiency (6,7). In general, however, conclusive assignment of diffusion changes observed with DWI to axonal and/or myelin damage is not straightforward, in part because the biophysics of diffusion *in vivo* is not fully understood and because axonal and myelin loss are histopathologically related. Additionally, the technique selected to analyze diffusion weighted images (DWIs) is an important consideration and has an impact on the quantitative interpretation of diffusion experiments. DWIs are typically analyzed with a mono-exponential tensor model that characterizes the observed signal decay according to the Stejskal-Tanner equation (8)

$$\ln(S/S_0) = -\gamma^2\delta^2(\Delta - \delta/3)\mathbf{G}\cdot\mathbf{D}\cdot\mathbf{G} = -\mathbf{b}:\mathbf{D} \quad [1]$$

where S/S_0 is the normalized signal intensity, γ is the proton gyromagnetic ratio, δ,G, and Δ are the duration, magnitude and leading edge separation time of the diffusion weighting gradient vector, respectively, and D is the diffusion tensor. Diffusion tensor imaging (DTI) has been applied in the brain (5,9–12) and spinal cord (10,13–15) and is typically performed in the low b-value (< 1500 s/mm^2) regime where the signal decay is, to a reasonable approximation, monoexponential. The degree to which diffusion is reduced in the CNS, compared to free water, is the result of micro-structural barriers, which generally includes multiple compartments *in vivo* and the diffusion time that molecules have to explore their environment. If restrictions between compartments are sufficiently large so that exchange is slow on the MR timescale, the signal attenuation will become non-monoexponential. This effect becomes apparent at higher b-values (> 1500 s/mm^2) in cell systems (16,17), animal models (18,19) and the human brain (20,21) and may be useful in detecting micro-structural changes due to WM damage. To improve the fit to the data, multi-component models can be used (19–22). Though bi-exponential fits approximate the observed signal behavior, a quantitative interpretation in terms of fast and slow diffusion components and corresponding assignment to extra- and intra-cellular water fractions has not been straightforward (19). This is not surprising, as cellular systems are comprised of many compartments of multiple sizes and shapes, many of which are connected through exchange. The use of relaxation agents in combination with diffusion studies (23) may aid the quantitative assignment of water diffusion populations.

An alternative approach to characterize diffusion is q-space analysis (24–27), which, unlike conventional DTI and DWI analysis, does not assume a Gaussian shape for the underlying probability density function (PDF) of molecular diffusion. The PDF is the conditional probability that a spin diffuses a distance $\mathbf{R} = \mathbf{r} - \mathbf{r_0}$ from its initial position $\mathbf{r_0}$ during the allowed diffusion time. At a given diffusion time, a tall, narrow PDF suggests a low diffusion constant and/or restricted diffusion, whereas a low, broad PDF suggests a high diffusion constant and/or more unrestricted diffusion. Q-space analysis allows experimental determination of the PDF and has been used in animal models to study the effects of reduced blood flow (28), myelin development (29), WM damage due to crush injury (30), myelin deficiency (31), and hypertension induced neurodegeneration (32). Structural information derived from q-space DWI in fixed rat spinal cords has also correlated well with axon diameters obtained from histological examination (33).

Recently, q-space DWI has been used to study experimental allergic encephalomyelitis in excised swine spinal cord (34) and multiple sclerosis (MS) in the human brain (35–37). MS is characterized by heterogeneous pathological changes in the CNS including demyelination, axonal loss and inflammation. Even though conventional MRI has emerged as a powerful tool to diagnose and prospectively monitor MS in clinical practice (38), some histopathological lesions appear normal on MRI examinations. To address this challenge, new MRI methods

have been developed to assess axonal damage and myelin loss, including magnetization transfer (MT) (39) and DWI techniques. MS involvement in the spinal cord is of particular interest because the prevalence of abnormalities is high (40) and because functional deficits can be associated with MRI indications of damage to the dorsal and lateral column WM, which convey sensory and motor information, respectively. The anatomical organization of the spinal cord, with densely packed, myelinated axons, oriented predominantly in one direction, makes it an ideal model system to investigate the effects of restricted diffusion. This *a priori* information allows diffusion weighting gradients to be oriented perpendicular to the WM fiber bundles, which is difficult to achieve in the brain due to its complex fiber architecture. The average diameter of axons in cervical spinal cord WM is approximately 1–1.5μm, increasing to approximately 1.7μm in MS lesions (40), which could be due to cell death of small axons and/or enlargement of surviving axons.

We hypothesized that the PDF of water diffusion perpendicular to the spinal cord's long axis may serve as a sensitive marker of disease-related damage. Here we demonstrate the ability of q-space DWI to delineate WM and gray matter (GM) and compare it to the apparent diffusion constant perpendicular to the WM fiber orientation ($ADC_{\perp}$), as well as to quantitative MT measurements.

MATERIALS AND METHODS

Theory

DWIs were acquired with a pulsed magnetic field gradient spin-echo (PGSE) experiment in which G is stepped while holding δ constant. The quantity $\mathbf{q} = \gamma\delta G/(2\pi)[\mathrm{cm}^{-1}]$ is independent of Δ, but the effective diffusion time $t_{dif} = \Delta - \delta/3$ should be stated for a given q-space experiment as it will affect the average displacement measured. The relationship between the measured signal attenuation $E_{tdif}(\mathbf{q})$, the PDF $\overline{P}_s(\mathbf{R},t_{dif})$, and the loss of phase coherence due to spin displacement is:

$$E_{tdif}(\mathbf{q}) = \int \overline{P}_s(\mathbf{R}, t_{dif}) \exp(i2\pi\mathbf{q}\cdot\mathbf{R}) d\mathbf{R} \quad [2]$$

The key principle in q-space analysis is that a Fourier transform (*FT*) of the signal attenuation with respect to **q** provides the PDF for diffusion:

$$\overline{P}_s(\mathbf{R}, t_{dif}) = FT\left\{E_{tdif}(q)\right\}. \quad [3]$$

The shape of the computed PDF can be characterized by the full width at half maximum (FWHM) and the maximum height (zero displacement probability, P_0) (29). In the specific case of unrestricted Gaussian diffusion, the diffusion constant *D* and the root mean square displacement (RMSD) for one-dimensional diffusion can be computed from the FWHM (27):

$$FWHM = 2\sqrt{4Dt_{dif}\ln(2)} \quad [4]$$

$$RMSD = \frac{FWHM}{2\sqrt{2\ln(2)}} = \sqrt{2Dt_{dif}}. \quad [5]$$

For consistency and ease of comparison with results from previous studies, the displacement values in this study are reported in terms of RMSD (0.425 × FWHM).

Subjects

The local institutional review board approved the study and informed consent was obtained from each subject. Eight healthy volunteers (6 males, 2 females, average age 32 ± 7 years) with no history of neurological disease and four individuals diagnosed with MS (two with relapsing remitting (RRMS) and two with secondary progressive (SPMS) forms of the disease) were enrolled in the study. Table 1 provides relevant clinical information. Follow-up datasets were acquired in 3 of the 4 patients as part of an ongoing longitudinal study.

MRI

Data were acquired on a 3T MR scanner (Philips Medical Systems, Best, The Netherlands), capable of producing 62mT/m magnetic field gradient strength. The body coil was used for transmission, while reception was accomplished with a 2-element surface coil placed bi-laterally around the neck. Pillows, sandbags and a head strap were used to minimize gross subject motion during scanning.

DWIs were acquired using spin-echo single-shot echo-planar imaging (EPI, SENSE factor = 1.8, TR/TE = 7000/112 ms). Thirty axial slices were acquired perpendicular to the long axis of the spinal cord covering approximately C1 to C7 (nominal resolution = 1.3 × 1.3 × 3.0 mm, field of view = 62 × 62 × 90 mm, scan matrix = 48 × 48, reconstructed matrix = 128 × 128). EPI-based geometric distortion can lead to anatomical mismatch between structural images and DWIs, especially in the spinal cord. To decrease the prevalence of susceptibility related artifacts, second order shimming was performed and a small acquisition matrix was used to decrease the length of the EPI echo train. To suppress foldover artifacts from surrounding tissue, saturation slabs were applied in the phase encoding direction (patient right-left axis) extending half the field of view outside the imaged volume. Diffusion weighting was applied perpendicular to the long axis of the spinal cord using both sets of transverse gradient coils to achieve the maximum gradient strength, thereby minimizing TE at the largest b-value. Gradient length (δ = 16ms) and leading edge spacing (Δ = 74.5ms) were kept constant, giving t_{dif} = 69.2ms. Gradient strength was increased up to G_{max} = 60.855 mT/m (b_{max} = 4685 s/mm^2) to achieve 31 linearly spaced q-values from 0 to 414 cm^{-1} (Table 2). The q-space DWI dataset was acquired in two separate blocks (b_0, b_1, b_3, b_5 … b_{29}) and (b_0, b_2, b_4, b_6 … b_{30}) where $b_{30} = b_{max}$ and b_0 is the k-space average of three scans with b = 0 s/mm^2. To improve SNR, each block was collected with diffusion weighting along two orthogonal directions ([G_x, G_y, G_z] = [1,1,0] and [1,−1,0]) with a total acquisition time of approximately 10 min.

Sagittal short-tau inversion recovery (STIR) images and high-resolution MT (41) datasets were also acquired for anatomical reference and lesion localization. For the latter, gradient echo volumes, consisting of 40 slices, were acquired with and without a 24ms sinc-shaped MT prepulse (8.5 μT played at 1.5 kHz off-resonance with respect to water at a nominal resolution of 0.69 × 0.69 × 2.25 mm). The acquisition with RF saturation is denoted as MT weighted (MTw). As reported previously (42), the MTw signal is largely sensitive to changes in macromolecular content (e.g. demyelination) and shows excellent contrast between healthy tissue and lesions in MS. Scan time for STIR and MT acquisitions was approximately 12 minutes.

Data Processing and Image Analysis

Processing was done offline on a Sun Fire V880 server (Sun Microsystems Inc., Santa Clara, CA). The b_0 images from all blocks were co-registered using FLIRT (FMRIB's Linear Image Registration Tool, Oxford, UK) (43) employing a rigid body 2 degrees of freedom (in plane

translation only) model. This restrictive model was selected because through-plane motion can be particularly difficult to identify in the spinal cord, especially in DWIs, which typically suffer from both low SNR and low tissue contrast. A further confounding factor is that the spinal cord, in contrast to the brain, has limited visual anatomical differences from slice to slice (given the limitations of MRI resolution). The same transformation was applied to the remaining DWIs of the same block. For each b-value, the coregistered images with G = [1,1,0] and [1,−1,0] were averaged to increase SNR. The four co-registered b_0 volumes were also averaged.

Q-space and statistical analyses were performed with in-house MATLAB (The Mathworks, Natick, MA) routines. For SNR calculations, average and difference images of DWIs with G = [1,1,0] and [1,−1,0] were computed at each b-value. The SNR was computed as the mean value in the dorsal column region of interest (ROI) in the average image divided by the standard deviation over the voxels in the same ROI within the difference image. For the data for q-space analysis (i.e. average of 4 b_0s and the average of 2 DWIs at each b-value), the mean SNR, averaged over the 8 controls and all slices, was 24±2:1, 8.8±1:1, 6.5±0.9:1 and 4±0.4:1 at b-values of 0, 83, 1020, and 4685 s/mm^2, respectively. For estimation of the noise floor, the standard deviation over all voxels in the difference image, at each b-value, was computed. The mean over a b-value range of 3519 to 4685 s/mm^2 was used as the noise floor and was subtracted from all data before processing. Signal falling below this artificial noise floor in magnitude images was set to zero. For each voxel, a bi-exponential fit was applied to the signal decay as a function of b-value for the sole purpose of extrapolating the signal decay to 1% of the value measured at b = 0 s/mm^2, to reduce truncation artifacts in the subsequent Fourier transform. The extrapolated signal decay was then zero-filled to q = 6150 cm^{-1} to improve resolution. The resulting curve was Fourier transformed with respect to q (Eq. 3), giving a PDF for each voxel. FWHM, P_0 and RMSD maps were computed on a voxel-by-voxel basis. In order to compare q-space and conventional DWI analysis, an $ADC_\perp$ map was computed by fitting the mono-exponential form of Eq. 1 to the signal attenuation at b-values up to 1020 s/mm^2.

Diffusion data were further analyzed by manually delineating ROIs in the dorsal column WM on the RMSD maps in each slice. Care was taken to exclude voxels of cerebrospinal fluid (defined as having a $ADC_\perp > 3$ μm^2/ms). It should be noted that, due to the small size of spinal cord structures with respect to the acquired resolution, some partial volume effects are unavoidable. These effects were reduced further by removing the outermost layer of voxels from the perimeter of each ROI. Each ROI consisted of approximately 60 to 70 voxels. The same ROIs were then applied to the P_0 and $ADC_\perp$ maps, and the mean value and standard deviation over all voxels within the ROIs were computed for the three contrasts.

To prevent anatomical mismatch (due to EPI-based image distortion) from confounding the comparison of results, MT data were coregistered and analyzed independently from the DWI data. The two volumes of the MT dataset were coregistered using a three degrees of freedom model (in plane translation and rotation) and were resliced, with sinc interpolation, to the match the number of slices and slice thickness of the DWI data. Magnetization transfer ratio (MTR) maps were computed on a voxel-by-voxel basis according to:

$$\mathrm{MTR} = 1 - \frac{S(\omega)}{S_0} \qquad [6]$$

where S_0 and $S(\omega)$ are the signal intensities in the absence and presence of RF irradiation, respectively. For MT analysis, a separate set of ROIs was manually delineated in the dorsal column WM on the MTw images. The ROIs were then applied to the MTR images and the mean value and standard deviation over all voxels within the ROIs were computed. The mean

MTw signal in each ROI was normalized by the mean CSF signal on the same slice in the MT image without RF saturation to provide MTCSF measurements (41).

Acquired data covered approximately the same anatomical extent of the cervical spinal cord in all subjects. To compare results across subjects, the resultant ROI-based RMSD, P_0, $ADC_\perp$, MTR and MTCSF data were normalized to a consistent anatomical coordinate system based on cervical vertebral levels. This was accomplished by identifying the slices at the superior aspect of the C2 and C6 vertebral bodies (anatomical landmarks) for each subject, as visualized on the overlay of the q-space DWI slice stack on the sagittal STIR image. Inspection of the data for 8 healthy controls showed that, on average, 21 slices were necessary to traverse the distance between these landmarks. Slices outside the landmarks were discarded as these areas were not visualized for all subjects. The mean and standard deviation values from the ROI-based analysis between the landmarks were interpolated to 21 equally spaced points spanning four complete vertebral segments (C2, C3, C4 and C5) and the RMSD, P_0, $ADC_\perp$, MTR and MTCSF results were partitioned accordingly. The average and standard deviation of the ROI-based measures from the eight controls were computed for each contrast and displayed as a function of slice level.

In addition to the voxel-by-voxel q-space analysis, PDFs and $ADC_\perp$ measurements were also obtained for ROIs in WM and MS lesions. This was done by computing the average diffusion weighted signal in each ROI as a function of b-value prior to taking the Fourier transform in q-space analysis and fitting for $ADC_\perp$.

Statistical Analysis

To determine the contrasts (RMSD, P_0, $ADC_\perp$, MTCSF and MTR) that show the most significant differences between MS patients and healthy controls, a slice-wise statistical analysis was performed. For each anatomically normalized slice level a distribution of approximately 600 data points was obtained by pooling the signal intensities from all voxels within each of the ROIs from all healthy controls. As the number of controls was small, this method provides a robust estimation of the true variance. At the same slice level, corresponding distributions were obtained for each MS patient (approximately 60 to 70 voxels per slice). Two-tailed and one-tailed Student's t-tests, assuming unequal variance, were performed to test the null hypothesis that the control distribution and distribution from a subject with MS had equal means (at a significance level of $\alpha = 0.01$). Separate tests were performed for each contrast at each anatomical slice level. An approximate measure of sensitivity to WM damage was defined as the number of slice levels (out of 21, expressed as a percentage) identified as significantly different from the control cohort. For the one-tailed t-tests, it was expected that RMSD, $ADC_\perp$, and MTCSF increase, while P_0 and MTR decrease in MS lesions.

RESULTS

Figure 1 shows typical DWIs as a function of b-value at the level of C4 in a healthy spinal cord. Because the diffusion weighting was applied perpendicular to the long axis of the spinal cord, WM signal is preserved even in the high b-value range, whereas GM signal drops off rapidly with b-value. Notably, the monoexponential fit, from which $ADC_\perp$ is calculated, describes the data well only at low b-values while the biexponential fit can fit the data reasonably well. The computed PDFs in WM are narrower and taller (decreased RMSD and increased P_0) than those for GM, and the GM horns and surrounding WM can be visually appreciated on the maps of RMSD and P_0.

Figure 2A shows three slices of the RMSD, P_0, and $ADC_\perp$ images for the healthy volunteer in Fig. 1. The GM-WM differentiation corresponds well to the anatomy shown in the MTw images at the same levels. As a first clinical example, RMSD, P_0 and $ADC_\perp$ images computed

for a 43-year old female with SPMS are also shown (Fig. 2B). There is a signal hyperintensity in the dorsal column on the MTw image. The RMSD and $ADC_{\perp}$ images also show hyperintensity, indicating increased diffusion in the transverse plane, whereas hypointensity is apparent on the P_0 image, indicating lower probability for no net water displacement during the diffusion time. Additionally, differential involvement in the right and left dorsal columns can be easily appreciated: an increased involvement of the right dorsal column is noted over the slices shown.

Figure 3 shows ROI-based q-space analysis for three slices through the dorsal column of the individual with SPMS shown in Figure 2. A qualitative decrease in tissue abnormality in the right dorsal column (red ROI and data) is noted in the panels from left to right (inferior to superior in the cord). It is readily apparent that the signal decay in grossly damaged WM (Panels D and E) is different from that observed in more normal-appearing WM (Panel F). The natural log of the signal attenuation as a function of b-value becomes more linear in regions of WM damage and approaches the mono-exponential fit. ROI-based PDFs are broader and lower in the lesion than in normal-appearing WM.

Figure 4 compares results from a healthy volunteer with those from a patient with RRMS with both lateral and dorsal column involvement as seen on the MTw images. The single-voxel PDFs illustrate the sensitivity of PDF shape to WM damage, which produces a broader, shorter PDF, approaching that of GM.

Figure 5 compares quantitative diffusion and MT measurements in ROIs in the dorsal column WM for 4 patients from the superior aspect of C2 to the superior aspect of C6. Areas of MS lesion involvement are indicated by increased RMSD, $ADC_{\perp}$, and MTCSF, and decreased P_0, relative to controls. MTR values were difficult to determine accurately, probably due to motion sensitivity in the ratio determination (note irregular values in Panels B and D, due to image artifacts), and did not change appreciably in most lesions due to the large error margins. The sensitivity of the q-space metrics to the presence of lesions is well demonstrated in Panel C where the deviation of $ADC_{\perp}$ relative to controls is minimal (well within one standard deviation), but quite noticeable (well outside one standard deviation) in RMSD and P_0 plots. Statistical analysis showed that, compared to $ADC_{\perp}$, ROI analysis of RMSD and P_0 identified more slices as significantly different from the control cohort (Table 3). While MTCSF proved to be quite sensitive to WM damage, the changes observed in MTR were generally small and within the standard deviation of controls, but at some locations appeared statistically significant due to the small standard deviation of MTR within an individual subject's ROI. Three of the four individuals with MS (Panels B, C, D) were scanned in a follow-up study, and good reproducibility of the q-space and $ADC_{\perp}$ results was found in all three instances. More detailed examinations of the reproducibility of results in healthy controls and correlations with MS disease progression in a longitudinal study are ongoing.

DISCUSSION

The results of this feasibility and initial clinical study show that it is possible to apply q-space imaging in the human cervical spinal cord *in vivo*, and that displacement (RMSD) and probability (P_0) maps provide useful contrasts to visualize spinal cord anatomy and WM damage. The degree to which diffusion is reduced in the CNS, compared to free water, is a product of micro-structural barriers, such as axonal and myelin membranes, as well as the experimentally chosen diffusion time that water molecules have to explore the local environment. These physical properties are conveyed in the diffusion properties measured perpendicular to the spinal cord's long axis with DTI (radial diffusion, $ADC_{\perp}$) or the RMSD and P_0 of the PDF in q-space DWI. The observed diffusivity is a complex combination of the volume fractions and diffusion constants of all compartments contributing to the voxel as well

as of the exchange occurring between them. Obviously, the number of observed quantities is too limited to draw many inferences about this microstructural environment. However, analytical models of restricted diffusion (22) have provided valuable insights into the interpretation of signal attenuation curves and allow extraction of some quantitative parameters.

Postmortem histopathology has shown marked morphological changes in spinal cords affected by MS, with increases in the mean axon diameter and axonal spacing, together with decreases in axon and myelin densities (40). These changes would necessarily affect the diffusion properties of water in the spinal cord. Even though precise correlations between diffusion measurements and morphology are not straightforward, DTI and the q-space approach can be used to obtain information about the average state of cellular systems and whether they are healthy or diseased. In healthy controls, PDFs in dorsal and lateral column WM (narrow, tall) are similar and are both distinct from the PDFs in GM (broad, short). When myelin and/or axonal damage occurs, the magnitude and number of restrictions is expected to decrease, resulting in increased diffusion. While the RMSD and P_0 can be expressed in terms of each other for a Gaussian PDF, this is not the case, in general, for non-Gaussian PDFs, and thus it is possible that the information provided by these contrasts could be different.

The results in this study showing that that the PDF shape is sensitive to WM damage, are consistent with previous studies in animals (29–32,34) and the human brain (35–37). However, we caution that comparison of quantitative values between *in vivo* studies and those using fixed tissue can only be qualitative, because tissue fixation and lower temperature will decrease the measured diffusion constant (44). The results for RMSD in healthy WM, and GM and in WM affected by MS are in good agreement with values reported in the literature (Table 4). Additionally, the observed increase in $ADC_\perp$ from 0.52–0.61±0.09 $\mu m^2/ms$ (across the C2 to C6 levels) in healthy WM to 0.65–1.0 $\mu m^2/ms$ in MS lesions (see Fig. 5) is in excellent agreement with the range of values reported for healthy WM (10,14,15) and the elevation of $ADC_\perp$ in the spinal cord (13) and corticospinal tract of patients with MS (45). Areas that appeared abnormal on q-space contrasts appeared abnormal (hyperintense) on the MTw images, which are sensitive to changes in macromolecular (i.e. myelin) content.

It is important to evaluate whether we have used sufficiently high b-values to reliably detect the slow diffusion component *in vivo*. Our results show that a departure from mono-exponential signal attenuation was apparent at $b > 1000\ s/mm^2$. This is in excellent agreement with Assaf et al (18) who showed detection of the slow diffusing component at $b > 1000\ s/mm^2$ in the rat spinal cord. These authors also reported, via simulation studies, that in heavily diffusion weighted images ($b > 2000\ s/mm^2$) the majority of the signal represents the slow diffusing component. Our DWIs at high b-value (Fig. 1) support this finding in that the signal in GM (predominantly monoexponential fast diffusion) is largely attenuated while signal in WM remains due to spatial restrictions.

Another important point is whether q-space analysis provides additional information or improved lesion detection compared to conventional measures of the fast diffusion component ($ADC_\perp$). Using the number of slices identified as significantly different from controls as an approximate measure of sensitivity to WM damage, statistical analysis showed that RMSD and P_0 were more sensitive to abnormal diffusion than $ADC_\perp$ (Table 3), even though it should be noted that the q-space dataset had inherently higher SNR due to the 10 minutes of data acquisition vs 5 minutes for the low b-value DWI dataset. While direct comparison of the sensitivity of diffusion and MTCSF measures to WM damage is not straightforward given the differences in resolution, SNR, and scan time, it is encouraging that the location and extent of WM damage compares favorably in both the images and the ROI analysis as a function of cervical level. Given the potential for detecting different pathological changes, a combined

MT and diffusion approach may be useful in quantitatively assessing WM damage in MS lesions. High b-value q-space DWI is well suited to evaluate WM damage through its effects on both the fast and slow diffusion components, which may provide different correlations with pathological changes.

Overall, the change in the shape of the PDF in MS lesions in the spinal cord can probably be explained by the loss of axonal and/or myelin barriers to diffusion, which offers the opportunity to use this technology to study the different pathologies presented by neurodegenerative diseases such as MS, and possibly amyotrophic lateral sclerosis and adrenoleukodystrophies.

Technical Considerations

The main drawback of q-space DWI is the requirement of heavy diffusion weighting, which reduces available SNR and may be impractical on some clinical scanners due to hardware limitations. This study, performed at 3T, benefited from the availability of a gradient strength of 62mT/m, permitting b-values of approximately 4700 s/mm^2 with a TE = 112 ms. This was possible even though the long TE and the high resolution needed to discern spinal cord structures limited SNR. This was accomplished by using a small field of view and a small imaging matrix, made possible by the availability of a phased-array surface coil setup to shorten the length of the EPI echo train (with the additional benefit of decreasing susceptibility related distortions). Previously, the effects of t_{dif}, δ and TE on q-space DWI indices have been investigated (46). Q-space theory requires $\delta \ll \Delta$, but this condition is difficult to fulfill on clinical scanners because the maximum magnetic field gradient strength is limited. Theoretical simulations (47) and studies in the rat spinal cord (46) and sciatic nerve (35) have shown that when δ is not negligible compared to Δ, the PDF obtained by q-space analysis is narrowed, resulting in an underestimate of the RMSD. Consequently, parameters derived from q-space DWI in this study should be interpreted as apparent values, and direct comparison between studies should be made with care.

A second condition in q-space analysis is that t_{dif} is long enough to allow spins sufficient time to encounter barriers to diffusion (i.e. $t_{dif} > a^2/2D$, where a is the compartment radius in the case of cylindrical symmetry). The average diameter of axons in healthy human spinal cord WM is approximately 1 to 1.5μm (40). Taking the diffusion constant of water to be approximately 2×10^{-9} m^2/s, the one-dimensional RMSD of a spin would exceed 1 μm after a t_{dif} of 0.25 ms. Thus the t_{dif} of 69ms in this study clearly satisfies the long diffusion time criterion. Previous studies have shown that while the PDF of perpendicular diffusion in mature rat spinal cord WM is largely independent of t_{dif}, diffusion in developing tissue is not (29). Consequently, improved GM-WM contrast has been demonstrated in the rat spinal cord by increasing t_{dif} (46). This approach may improve detection of WM damage, where diffusion is less restricted, and longer diffusion times could be achieved by the use of stimulated echo sequences. At the cost of increased scan time, additional SNR could be achieved by increasing the number of averages and implementing appropriate cardiac gating to minimize instability-based noise due to cardiac pulsation and respiratory motion. It is also feasible that the total scan time for a q-space DWI dataset could be reduced by acquiring DWIs at fewer b-values and employing a fitting and interpolation procedure. It is tremendously encouraging that DWIs of the quality reported here can be obtained even without these additional considerations in a scan time that is clinically feasible.

CONCLUSION

Diffusion-weighted imaging with q-space analysis can be used to study the diffusion properties of water in the human spinal cord *in vivo* in both healthy and diseased tissue.

Acknowledgments

We are grateful to Ms. Terri Brawner, Ms. Kathleen Kahl and Ms. Ivana Kusevic for their help with data acquisition and to Mr. Joseph Gillen and Dr. Susumu Mori for invaluable discussions and technical assistance. This publication was made possible by Grant Number P41 RR015241 from the National Center for Research Resources (NCRR), a component of the National Institutes of Health (NIH). Its contents are solely the responsibility of the authors and does not necessarily represent the official view of NCRR or NIH. Dr. Peter C.M. van Zijl is a paid lecturer for Philips Medical Systems. This arrangement has been approved by Johns Hopkins University in accordance with its conflict of interest policies.

Grant Support:

NIH/NCRR P41RR15241; National MS Society CA 1029-A-2, TR-3760-A-3; NIH AG20012; Nancy Davis Center without Walls.

REFERENCES

1. Beaulieu C. The basis of anisotropic water diffusion in the nervous system - a technical review. NMR Biomed 2002;15(7–8):435–455. [PubMed: 12489094]
2. Chenevert TL, Brunberg JA, Pipe JG. Anisotropic diffusion in human white matter: demonstration with MR techniques in vivo. Radiology 1990;177(2):401–405. [PubMed: 2217776]
3. Le Bihan D. Molecular diffusion, tissue microdynamics and microstructure. NMR Biomed 1995;8(7–8):375–386. [PubMed: 8739274]
4. Moseley ME, Cohen Y, Kucharczyk J, Mintorovitch J, Asgari HS, Wendland MF, Tsuruda J, Norman D. Diffusion-weighted MR imaging of anisotropic water diffusion in cat central nervous system. Radiology 1990;176(2):439–445. [PubMed: 2367658]
5. Horsfield MA, Jones DK. Applications of diffusion-weighted and diffusion tensor MRI to white matter diseases - a review. NMR Biomed 2002;15(7–8):570–577. [PubMed: 12489103]
6. Song SK, Sun SW, Ramsbottom MJ, Chang C, Russell J, Cross AH. Dysmyelination revealed through MRI as increased radial (but unchanged axial) diffusion of water. Neuroimage 2002;17(3):1429–1436. [PubMed: 12414282]
7. Song SK, Yoshino J, Le TQ, Lin SJ, Sun SW, Cross AH, Armstrong RC. Demyelination increases radial diffusivity in corpus callosum of mouse brain. Neuroimage 2005;26(1):132–140. [PubMed: 15862213]
8. Stejskal EO, Tanner JE. Spin Diffusion Measurements: Spin Echoes in the Presence of a Time-Dependent Field Gradient. J Chem Phys 1965;42(1):288–292.
9. Basser PJ, Jones DK. Diffusion-tensor MRI: theory, experimental design and data analysis - a technical review. NMR Biomed 2002;15(7–8):456–467. [PubMed: 12489095]
10. Clark CA, Werring DJ. Diffusion tensor imaging in spinal cord: methods and applications - a review. NMR Biomed 2002;15(7–8):578–586. [PubMed: 12489104]
11. Le Bihan D, van Zijl P. From the diffusion coefficient to the diffusion tensor. NMR Biomed 2002;15(7–8):431–434. [PubMed: 12489093]
12. Mori S, van Zijl PC. Fiber tracking: principles and strategies - a technical review. NMR Biomed 2002;15(7–8):468–480. [PubMed: 12489096]
13. Clark CA, Werring DJ, Miller DH. Diffusion imaging of the spinal cord in vivo: estimation of the principal diffusivities and application to multiple sclerosis. Magn Reson Med 2000;43(1):133–138. [PubMed: 10642740]
14. Holder CA, Muthupillai R, Mukundan S Jr, Eastwood JD, Hudgins PA. Diffusion-weighted MR imaging of the normal human spinal cord in vivo. AJNR Am J Neuroradiol 2000;21(10):1799–1806. [PubMed: 11110530]
15. Ries M, Jones RA, Dousset V, Moonen CT. Diffusion tensor MRI of the spinal cord. Magn Reson Med 2000;44(6):884–892. [PubMed: 11108625]
16. Latour LL, Svoboda K, Mitra PP, Sotak CH. Time-dependent diffusion of water in a biological model system. Proc Natl Acad Sci U S A 1994;91(4):1229–1233. [PubMed: 8108392]

17. Van Zijl PC, Moonen CT, Faustino P, Pekar J, Kaplan O, Cohen JS. Complete separation of intracellular and extracellular information in NMR spectra of perfused cells by diffusion-weighted spectroscopy. Proc Natl Acad Sci U S A 1991;88(8):3228–3232. [PubMed: 2014244]
18. Assaf Y, Cohen Y. Assignment of the water slow-diffusing component in the central nervous system using q-space diffusion MRS: implications for fiber tract imaging. Magn Reson Med 2000;43(2): 191–199. [PubMed: 10680682]
19. Niendorf T, Dijkhuizen RM, Norris DG, van Lookeren Campagne M, Nicolay K. Biexponential diffusion attenuation in various states of brain tissue: implications for diffusion-weighted imaging. Magn Reson Med 1996;36(6):847–857. [PubMed: 8946350]
20. Clark CA, Le Bihan D. Water diffusion compartmentation and anisotropy at high b values in the human brain. Magn Reson Med 2000;44(6):852–859. [PubMed: 11108621]
21. Mulkern RV, Gudbjartsson H, Westin CF, Zengingonul HP, Gartner W, Guttmann CR, Robertson RL, Kyriakos W, Schwartz R, Holtzman D, Jolesz FA, Maier SE. Multi-component apparent diffusion coefficients in human brain. NMR Biomed 1999;12(1):51–62. [PubMed: 10195330]
22. Stanisz GJ, Szafer A, Wright GA, Henkelman RM. An analytical model of restricted diffusion in bovine optic nerve. Magn Reson Med 1997;37(1):103–111. [PubMed: 8978638]
23. Silva MD, Omae T, Helmer KG, Li F, Fisher M, Sotak CH. Separating changes in the intra- and extracellular water apparent diffusion coefficient following focal cerebral ischemia in the rat brain. Magn Reson Med 2002;48(5):826–837. [PubMed: 12417997]
24. Callaghan P, Codd S, Seymour J. Spatial Coherence Phenomena Arising from Translational Spin Motion in Gradient Spin Echo Experiments. Concepts Magn Reson 1999;11:181–202.
25. Callaghan P, Coy A, MacGowan D, Packer K, Zelaya F. Diffraction-like effects in NMR diffusion studies of fluid in porous solids. Nature 1991;351:467–469.
26. Cohen Y, Assaf Y. High b-value q-space analyzed diffusion-weighted MRS and MRI in neuronal tissues - a technical review. NMR Biomed 2002;15(7–8):516–542. [PubMed: 12489099]
27. Cory DG, Garroway AN. Measurement of translational displacement probabilities by NMR: an indicator of compartmentation. Magn Reson Med 1990;14(3):435–444. [PubMed: 2355827]
28. King MD, Houseman J, Gadian DG, Connelly A. Localized q-space imaging of the mouse brain. Magn Reson Med 1997;38(6):930–937. [PubMed: 9402194]
29. Assaf Y, Mayk A, Cohen Y. Displacement imaging of spinal cord using q-space diffusion-weighted MRI. Magn Reson Med 2000;44(5):713–722. [PubMed: 11064406]
30. Nossin-Manor R, Duvdevani R, Cohen Y. q-Space high b value diffusion MRI of hemi-crush in rat spinal cord: evidence for spontaneous regeneration. Magn Reson Imaging 2002;20(3):231–241. [PubMed: 12117605]
31. Biton IE, Duncan ID, Cohen Y. High b-value q-space diffusion MRI in myelin-deficient rat spinal cords. Magn Reson Imaging 2006;24(2):161–166. [PubMed: 16455404]
32. Assaf Y, Mayk A, Eliash S, Speiser Z, Cohen Y. Hypertension and neuronal degeneration in excised rat spinal cord studied by high-b value q-space diffusion magnetic resonance imaging. Exp Neurol 2003;184(2):726–736. [PubMed: 14769364]
33. Bar-Shir A, Cohen Y. High b-value q-space diffusion MRS of nerves: structural information and comparison with histological evidence. NMR Biomed. 2007 May 9; Published online in advance of print. DOI:10.1002/nbm.1175.
34. Biton IE, Mayk A, Kidron D, Assaf Y, Cohen Y. Improved detectability of experimental allergic encephalomyelitis in excised swine spinal cords by high b-value q-space DWI. Exp Neurol 2005;195 (2):437–446. [PubMed: 16098966]
35. Assaf Y, Ben-Bashat D, Chapman J, Peled S, Biton IE, Kafri M, Segev Y, Hendler T, Korczyn AD, Graif M, Cohen Y. High b-value q-space analyzed diffusion-weighted MRI: application to multiple sclerosis. Magn Reson Med 2002;47(1):115–126. [PubMed: 11754450]
36. Assaf Y, Chapman J, Ben-Bashat D, Hendler T, Segev Y, Korczyn AD, Graif M, Cohen Y. White matter changes in multiple sclerosis: correlation of q-space diffusion MRI and 1H MRS. Magn Reson Imaging 2005;23(6):703–710. [PubMed: 16198825]
37. Latt J, Nilsson M, Wirestam R, Johansson E, Larsson EM, Sta hlberg F, Brockstedt S. In vivo visualization of displacement-distribution-derived parameters in q-space imaging. Magn Reson Imaging. 2007 June 18; Published online in advance of print. DOI:10.1016/j.mri.2007.04.001.

38. Arnold DL. Matthews PM. MRI in the diagnosis and management of multiple sclerosis. Neurology 2002;58(8 Suppl 4):S23–S31. [PubMed: 11971123]
39. Henkelman RM, Stanisz GJ, Graham SJ. Magnetization transfer in MRI: a review. NMR Biomed 2001;14(2):57–64. [PubMed: 11320533]
40. Bot JC, Blezer EL, Kamphorst W, Lycklama ANGJ, Ader HJ, Castelijns JA, Ig KN, Bergers E, Ravid R, Polman C, Barkhof F. The spinal cord in multiple sclerosis: relationship of high-spatial-resolution quantitative MR imaging findings to histopathologic results. Radiology 2004;233(2):531–540. [PubMed: 15385682]
41. Smith SA, Golay X, Fatemi A, Jones CK, Raymond GV, Moser HW, van Zijl PC. Magnetization transfer weighted imaging in the upper cervical spinal cord using cerebrospinal fluid as intersubject normalization reference (MTCSF imaging). Magn Reson Med 2005;54(1):201–206. [PubMed: 15968676]
42. Fatemi A, Smith SA, Dubey P, Zackowski KM, Bastian AJ, van Zijl PC, Moser HW, Raymond GV, Golay X. Magnetization transfer MRI demonstrates spinal cord abnormalities in adrenomyeloneuropathy. Neurology 2005;64(10):1739–1745. [PubMed: 15911801]
43. Jenkinson M, Bannister P, Brady M, Smith S. Improved optimization for the robust and accurate linear registration and motion correction of brain images. NeuroImage 2002;17(2):825–841. [PubMed: 12377157]
44. Sun SW, Neil JJ, Liang HF, He YY, Schmidt RE, Hsu CY, Song SK. Formalin fixation alters water diffusion coefficient magnitude but not anisotropy in infarcted brain. Magn Reson Med 2005;53(6): 1447–1451. [PubMed: 15906292]
45. Reich DS, Smith SA, Zackowski KM, Gordon-Lipkin EM, Jones CK, Farrell JA, Mori S, van Zijl PC, Calabresi PA. Multiparametric magnetic resonance imaging analysis of the corticospinal tract in multiple sclerosis. Neuroimage 2007;38(2):271–279. [PubMed: 17870615]
46. Nossin-Manor R, Duvdevani R, Cohen Y. Effect of experimental parameters on high b-value q-space MR images of excised rat spinal cord. Magn Reson Med 2005;54(1):96–104. [PubMed: 15968658]
47. Mitra PP, Halperin BI. Effects of finite gradient-pulse widths in pulsed-field-gradient diffusion measurements. J Magn Reson A 1995;113(1):94–101.

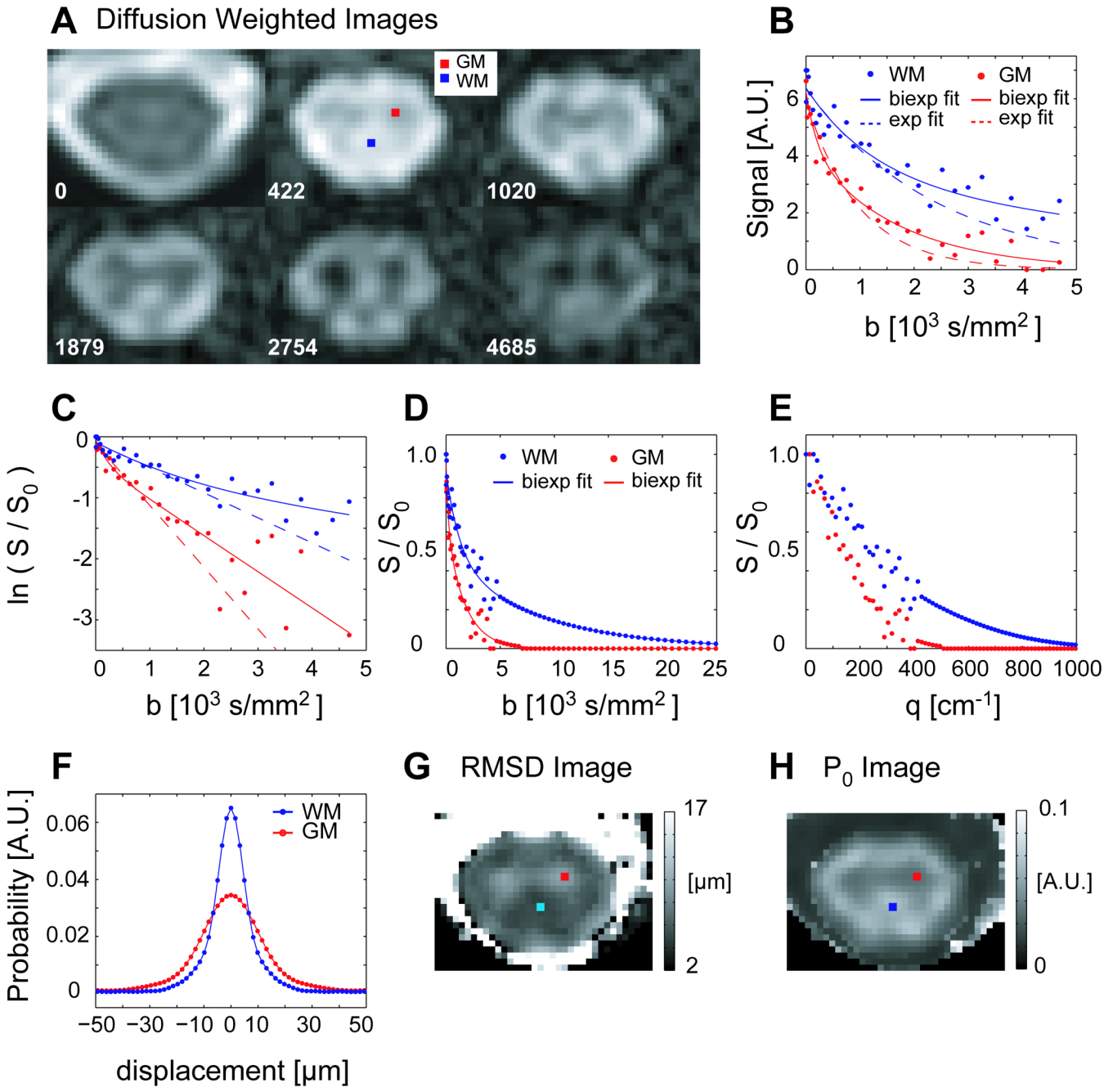

Figure 1.

A) DWIs (axial cross section, average of 2 diffusion weighting directions) through C4 spinal cord in a healthy 25 year old female volunteer. All DWIs (b>0) have the same windowing level. **B)** Measured signal decays for representative WM and GM voxels as a function of b-value, with bi-exponential (solid line) and mono-exponential (dashed line) fits. **C)** Natural log of the normalized signal showing departure from mono-exponential signal attenuation. **D, E)** The normalized signal, extrapolated and zero-padded (partial) data series as a function of b- and q- value, respectively. **F)** PDFs computed for GM and WM voxels. **G, H)** Maps of the RMSD and height (P_0) of the PDF computed for each voxel at the slice level, with the location of the representative voxels indicated.

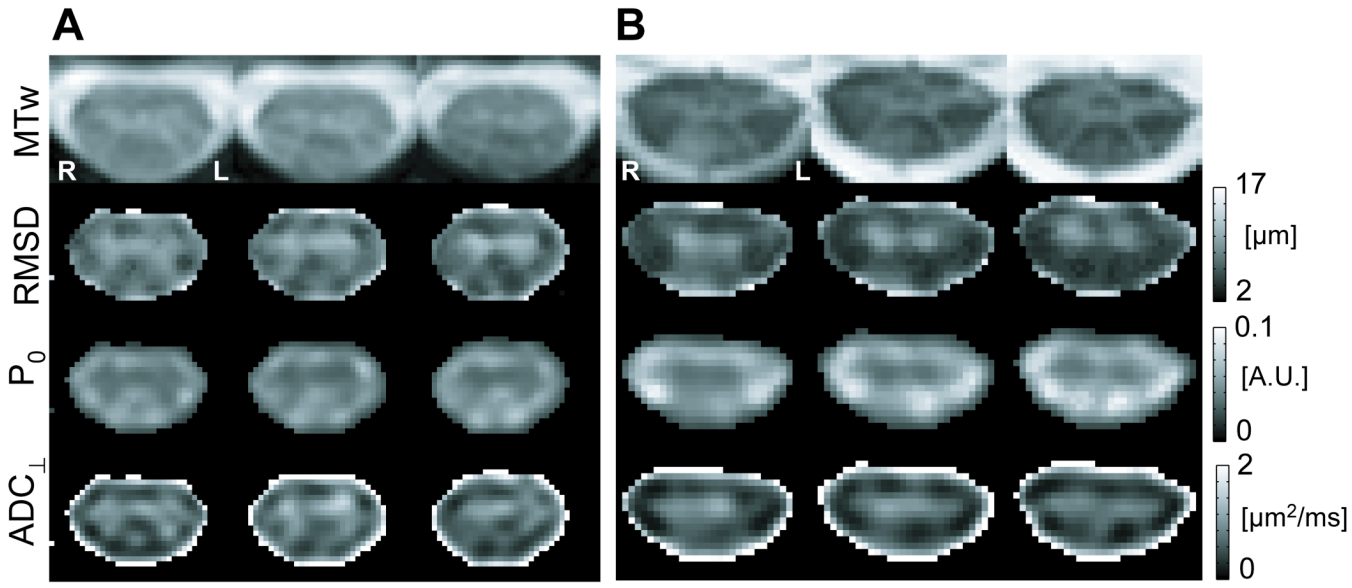

Figure 2.

Comparison of MTw, RMSD, P_0, and $ADC_\perp$ maps. **A)** The healthy female volunteer in Figure 1. Three contiguous slices from C5 to C4 shown (left to right) clearly demonstrate the shape of the GM horns and surrounding WM in all image types. **B)** 43 year old female with SPMS. Contiguous slices extending from C4 to approximately mid level of C3 (left to right in the figure). On all four images, MS-related abnormality in the right dorsal column is evident. For visual display, voxels outside the cord are set to zero for the RMSD, P_0 and $ADC_\perp$ maps.

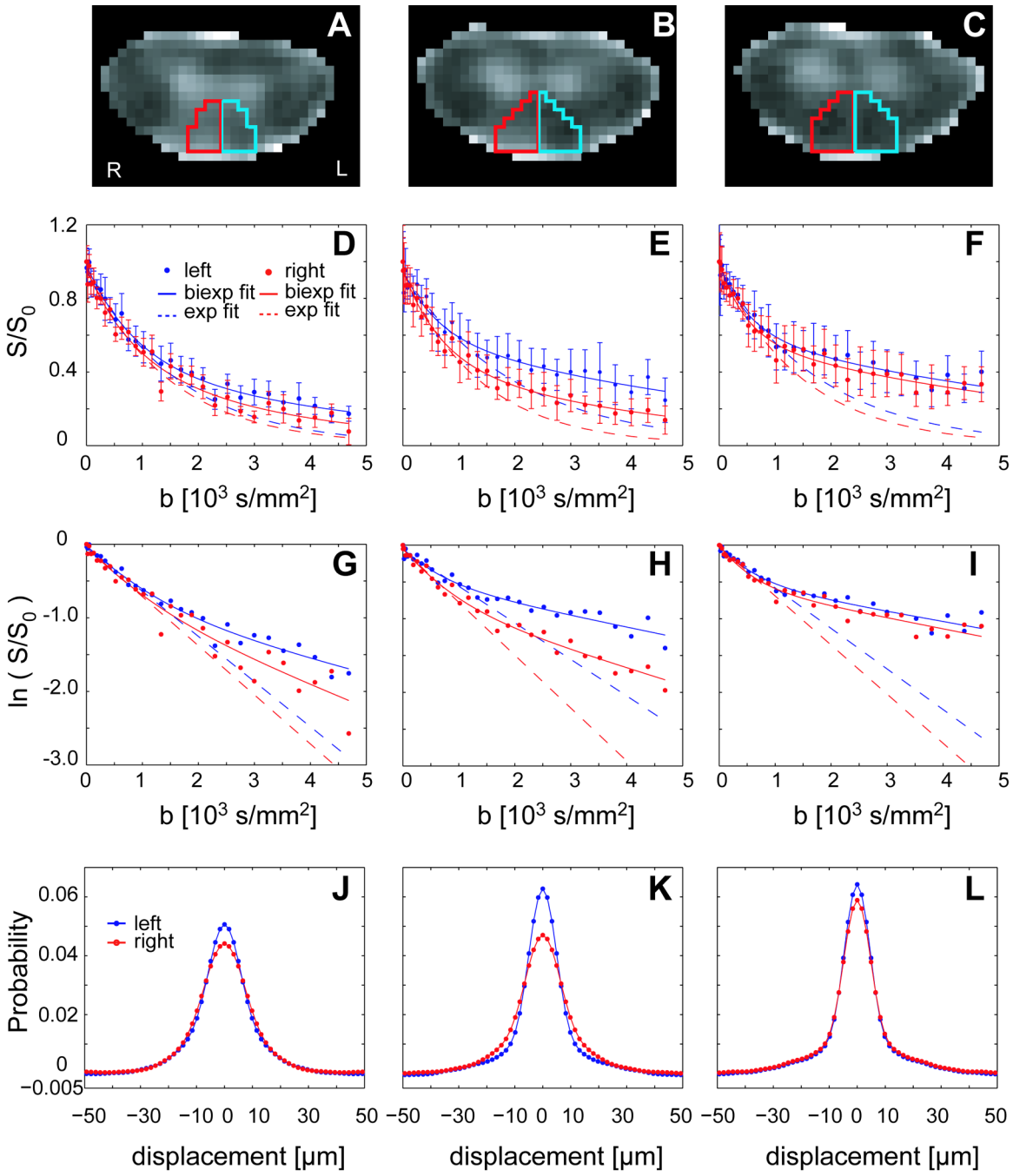

Figure 3.
ROI analysis for the three contiguous slices for the SPMS patient in Figure 2. **A–C)** ROI definition in the right (red) and left (blue) dorsal columns overlaid on RMSD images. **D–F)** Average signal intensity (± SD over ROI voxels) plotted as a function of b-value. **G–I)** The natural log of average signal intensity as a function of b-value. **J–L)** computed PDFs.

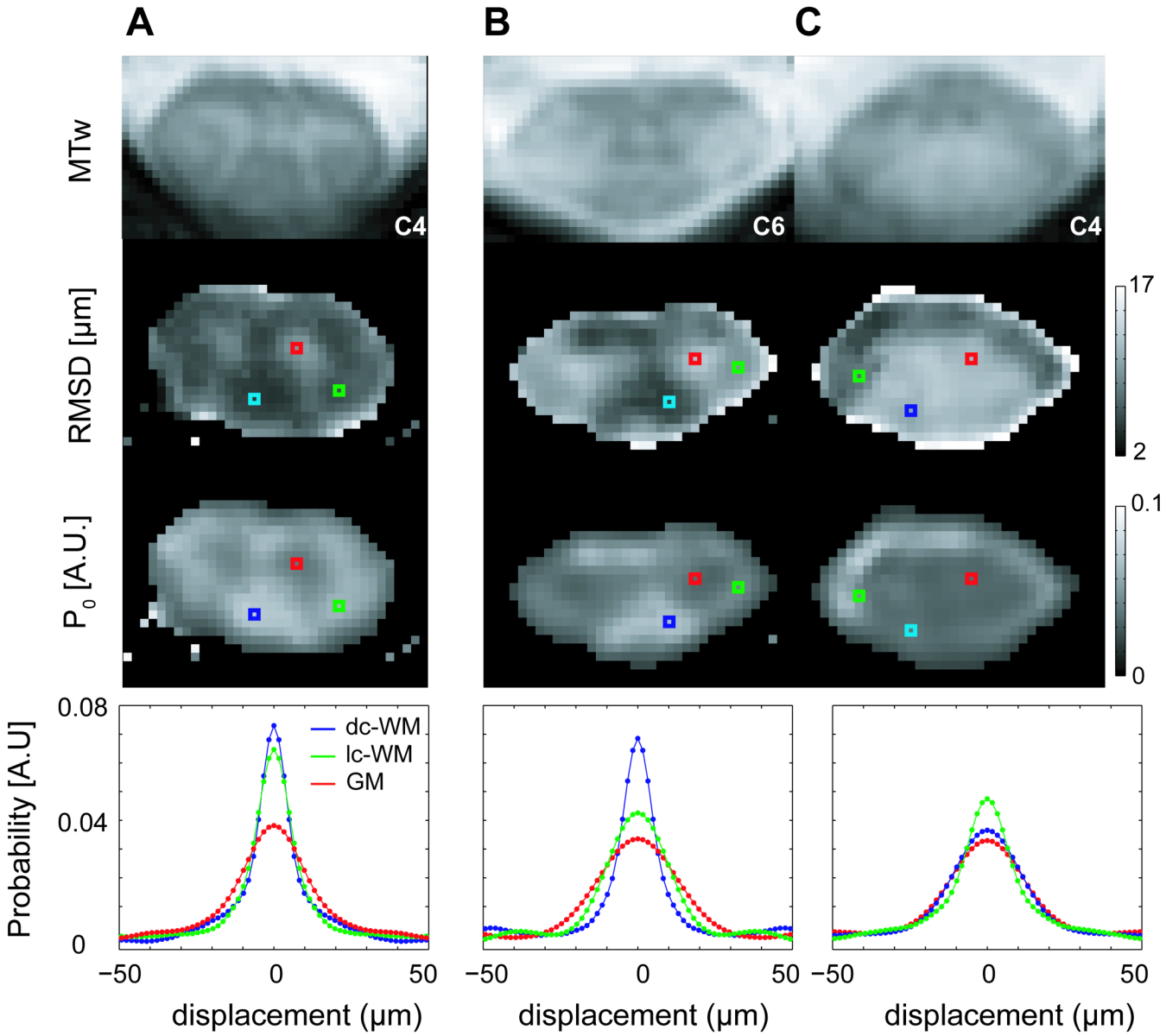

Figure 4.

MTw, RMSD, and P_0 images and voxel-based PDFs for a healthy 25-year old male volunteer at the C4 level (**A**) and for a 25 year old male with RRMS at slice levels C6 **(B)** and C4 **(C)**. Lesion involvement in the lateral (lc-WM) and dorsal column WM (dc-WM) is visible, with lesions appearing hyperintense on the RMSD image, hypointense on the P_0 image, and hyperintense on the MTw image.

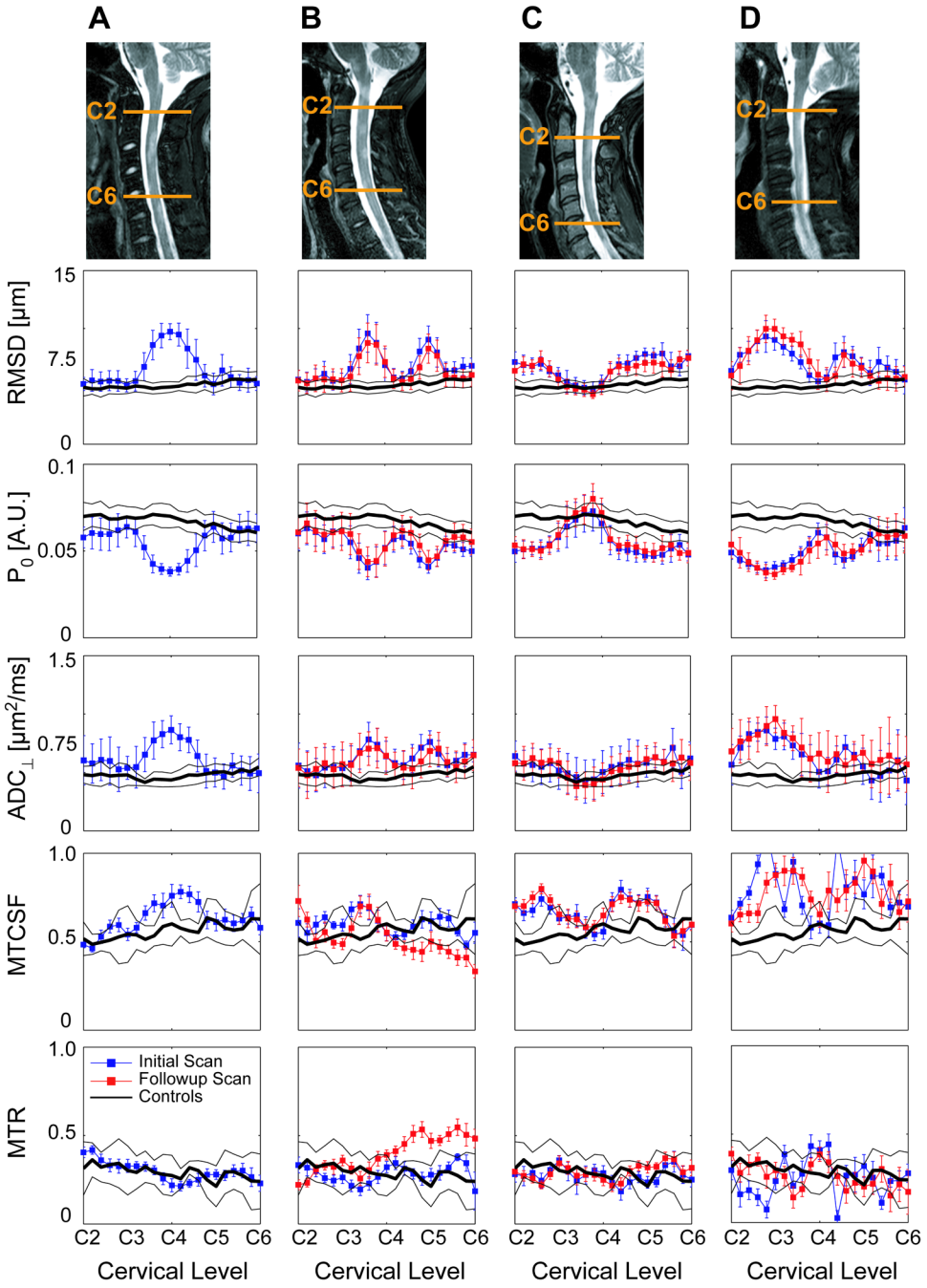

Figure 5.

RMSD, P_0, $ADC_\perp$, MTCSF and MTR within ROIs in the dorsal column WM (mean ± standard deviation over the voxels in the ROI), plotted as a function of cervical level. Results for four patients, **A)** 25 year old male with RRMS, **B)** 31 year old female with RRMS, **C)** 43 year old female with SPMS and **D)** 41 year old male with SPMS, are compared with the average results (solid black line, ± one standard deviation) from 8 healthy controls. Initial and follow-up results are shown for three of the MS patients. Sagittal STIR images show slice and lesion localization for the initial exam of each patient.

Table 1

Clinical information for patients studied

Patient	MS Subtype	Age (years)	Gender	Evaluations	Disease Duration (years)	EDSS	Affected Systems (FSS>= 2)
A	RR	25	male	initial	1	3.5	V, C, B
B	RR	31	female	initial	8	3.5	P, C, B, S
				4 months	8	5.5	P, C, B
C	SP	43	female	initial	15	3.5	P, C
				4 months	15	3.5	P, C
D	SP	41	male	initial	6	5.5	P, C, S, CL
				2 months	6	5.5	P, C, S, CL

Expanded disability status scale (EDSS); functional system score (FSS). Affected system abbreviations: visual (V), cerebellar (C), bowel and bladder (B), pyramidal (P), sensory (S), cerebral (CL)

Table 2

Acquired b-values and corresponding q-values at t_{dif} = 69.2ms

b-value s/mm^2	q-value cm^{-1}	b-value s/mm^2	q-value cm^{-1}
0	0.0	1333	220.9
5	13.8	1504	234.7
21	27.6	1687	248.5
47	41.4	1879	262.3
83	55.2	2082	276.2
130	69.0	2296	290.0
187	82.8	2520	303.8
255	96.7	2754	317.6
333	110.5	2998	331.4
422	124.3	3254	345.2
521	138.1	3519	359.0
630	151.9	3795	372.8
750	165.7	4081	386.6
880	179.5	4378	400.4
1020	193.3	4685	414.2
1171	207.1		

Table 3

Percentage of anatomical slice levels (out of 21 slices) identified as significantly different from controls at a significance level of $\alpha = 0.01$.

	Percent of slices significantly different from controls							
Patient	**A**		**B**		**C**		**D**	
t-test type	**Two|**	**one sided**	**Two**	**one sided**	**Two**	**one sided**	**Two**	**one sided**
RMSD	76	67	93	93	86	79	86	86
P_0	71	71	95	95	83	79	86	86
$ADC_\perp$	67	62	86	86	55	50	79	76
MTCSF	86	76	90	43	95	81	95	93
MTR	86	52	88	43	79	57	88	57

Results from initial and follow-up evaluations are averaged. Values are reported for two-sided and one-sided t-tests for the four cases (A–D) shown in Figure 5.

Table 4

RMSD values for diffusion measured perpendicular to the long axis of WM fibers in the brain and spinal cord with q-space DWI.

Study Type	RMSD (μm)			δ/t_{dif} (ms)	Disease / Model	Ref.
	WM Control	GM Control	WM Lesion			
Human[a]						
Spinal Cord	5.2–6.3 ± 0.9[+]	8.5–10	7–10	16/69	MS	This study
Brain	9	11.9[*]	13	20/81	MS	(37)
Brain	3.8 ± 0.2	5–9	6.9 ± 0.6	65/49	MS	(36)
Brain	3.3 ± 0.8	7–9	8.1 ± 2.4	65/49	MS	(35)
Swine						
Spinal Cord[c]	5.83 ± 0.06[*]	7–8[†]	7.3 ± 0.4[*]	10/200	EAE	(34)
Rat						
Spinal Cord[b]	2–3	9–10	6.6 ± 0.6[‡]	2/150	Development	(29)
Spinal Cord[c]	2.2 ± 0.3	6.1 ± 1.3	3.8 ± 0.6	2/150	Hypertension	(32)
Spinal Cord[d]	6.6 ± 0.1[†]	8.2 ± 0.6[†]	7.5 ± 0.5[†]	2/50	Myelin deficient	(31)
Spinal Cord[d]	2.7 ± 0.1	9.7 ± 0.3	3.9 ± 0.3	2/150	Crush trauma	(30)

[a] *in vivo* studies.

[b] Excised tissue, no fixation.

[c] Formalin fixed tissue,

[d] paraformaldehyde fixed tissue.

[+] across the C2 to C6 levels,

[*] computed from data in supplied tables.

[†] estimated from figure.

[‡] 7 day old rat (compared to WM and GM control in 77 day old mature rat).

Experimental allergic encephalomyelitis (EAE).